ICES Journal of Marine Science

ICES Journal of Marine Science (2018), 75(3), 1117–1130. doi:10.1093/icesjms/fsx206

Original Article

Deep-water calibration of echosounders used for biomass surveys and species identification

Kunnath Haris*, Rudy J. Kloser, Tim E. Ryan, and Jacques Malan

CSIRO Oceans and Atmosphere, GPO Box 1538, Hobart, Tasmania 7001, Australia

**Corresponding author: e-mail: haris.kunnath@csiro.au.*

Haris, K., Kloser, R. J., Ryan, T. E., and Malan, J. Deep-water calibration of echosounders used for biomass surveys and species identification. – ICES Journal of Marine Science, 75: 1117–1130.

Received 26 July 2017; revised 13 October 2017; accepted 13 October 2017; advance access publication 2 December 2017.

Acoustic quantification of aquatic biomass using echosounders requires accurate calibration. With the advancing applications of deep-water echosounders involving moored, towed, profiling and autonomous instruments, calibration of echosounders at the operating depth is needed to ensure unbiased estimates of biomass and species identification. In this context, the deepwater calibration acoustic facility (DeCAF) was used to examine the depth-dependent variations in on-axis gain (G_0) and equivalent two-way beam angle (Ψ) of three different transducers, operating at 38 (Simrad ES38-DD and MSI-38) and 120 kHz (Simrad ES120-7CD) used for biomass surveys and species identification. The analyses carried out using the sphere calibration method reveal significant variations in calibrated G_0 and Ψ that in combination could result in substantial systemic biases in quantitative biomass estimation and species identification. The depth-dependent G_0 variations derived using the DeCAF system are in accordance with available deep-water calibration results, demonstrating reasonable repeatability of target strength measurements ($\pm$0.6 dB) over the calibration deployments. Importantly, Ψ of the transducers was calculated to be consistently lower than the values specified by the manufacturer, and for one transducer would result in 18% change in the estimated biomass. These results highlight the potential for bias if the Ψ of transducer is not independently calculated using the actual survey echosounder.

Keywords: acoustics, calibration, deep-water, echosounder, split-beam.

Introduction

Echosounder calibration is a fundamental requirement in quantitative aquatic biomass surveys and species identification (Simmonds and MacLennan, 2005). Traditionally, surveys have been conducted using hull-mounted transducers, but increasingly echosounders are being used on "deeply" moored (Brierley *et al.*, 2006; Doksæter *et al.*, 2009; Kaartvedt *et al.*, 2009; Urmy *et al.*, 2012; Godø *et al.*, 2013), towed (Dalen and Bodholt, 1991; Kloser, 1996; Kloser *et al.*, 2002, 2013; Dalen *et al.*, 2003; Ryan *et al.*, 2009; O'Driscoll *et al.*, 2013), profiling (Ona, 2003; Kloser *et al.*, 2009; Pedersen *et al.*, 2011; Kloser *et al.*, 2016), and autonomous (Godø and Totland, 1996; Fernandes *et al.*, 2003; Patel *et al.*, 2004; Moline *et al.*, 2015) systems to investigate biomass and species composition of deep-water ecosystems. Acoustic observations from deep-water echosounders on a range of platforms can advance our understanding of deep-water ecosystems (Handegard *et al.*, 2013). In this context, *in situ* calibrations of these instruments are required to reduce the bias in estimates of biomass and to improve species identification. Calibration of acoustic systems involves primary calculations of two performance parameters: (i) the transducer on-axis gain G_0 (dB re 1), and (ii) the equivalent two-way beam angle Ψ (dB re 1 sr) of the transducer beam pattern $B(\alpha, \beta)$ (dB re 1) (Demer *et al.*, 2015).

The overall on-axis performance of echosounders can be evaluated by the established sphere calibration method (Demer *et al.*, 2015). This method provides calibrated G_0 values and commonly used to monitor on-axis performance of hull-mounted split-beam echosounders (Knudsen, 2009). However, in deep-water systems the G_0 parameters that account for the corresponding twofold variations in the measured target strength (TS) (dB re 1 m^2) may vary as a function of operating depth (Kloser, 1996; Dalen *et al.*, 2003; Ryan *et al.*, 2009; Pedersen *et al.*, 2011;

O'Driscoll *et al.*, 2013) and environmental parameters (Demer and Hewitt, 1992; Brierley *et al.*, 1998; Demer and Renfree, 2008). Therefore, it is important to calibrate echosounders over the range of environmental conditions (i.e. temperature, salinity, and pressure) encountered during the biomass survey.

The Ψ of transducers is an important (and apparently the least investigated) calibration parameter in echo-integration based biomass estimation. Incorrect Ψ values contribute to a first-order bias in a biomass estimate (Reynisson, 1998; Demer, 2004). The Ψ is estimated by comprehensive mapping of the transducer $B(\alpha, \beta)$ by rotating the mounting arrangement (Simmonds, 1984, 1990), repositioning the calibration sphere (Reynisson, 1986, 1990, 1998; Kieser and Ona, 1988; Brede *et al.*, 1990; Ona, 1990; Vagle *et al.*, 1996), or both (Jech *et al.*, 2005), and trimming of the vessel above calibration sphere (Ona and Vestnes, 1985). It is often assumed that the manufacturer-specified Ψ' (dB re 1 sr) (adjusting for the difference in sound speed) is correct due to the difficulty in obtaining an independent measurement. However, discrepancies have been observed between calculated Ψ and Ψ' values (Simmonds, 1990; Reynisson, 1998), necessitating the requirement to determine the correct value of Ψ, and examine its depth-dependent variations for each transducer used in the biomass survey.

In this context, we used the deepwater calibration acoustic facility (DeCAF) that was specifically developed to characterize the depth-dependent variations in G_0 and $B(\alpha, \beta)$ of deeply deployed split-beam echosounders down to 1500 m (Malan *et al.*, 2016). This development overcomes previous limitations of deep-water echosounder calibration where it was difficult to maintain the target sphere on-axis due to currents and misalignment of the platform (Kloser, 1996; Ryan *et al.*, 2009). Using the DeCAF platform, it is now possible to independently verify $B(\alpha, \beta)$ of the transducers and its depth-dependent variations in the survey area.

In this article, we calibrated three deep-water scientific split-beam echosounders to determine how the echosounder on-axis sensitivity changes with depth over multiple deployments. Moreover, we measured the transducer $B(\alpha, \beta)$ and derived Ψ variation as a function of operating depth.

Methods

Calibration deployments

The DeCAF system was used to calibrate three transducers (Table 1) simultaneously from the surface down to 800 m water depth (Malan *et al.*, 2016). The DeCAF deployments (IN 2015-E03, OD 2015, and IN 2016-E02) were conducted in suitable weather conditions to minimize platform movement with $B(\alpha, \beta)$ measurements at 100 m depth intervals (Figure 1).

The extension arms of DeCAF (Figure 2a) were used to suspend a 38.1 mm diameter calibration sphere (made from tungsten carbide with 6% cobalt binder material, WC) and a 10 kg ballast weight by conjoining three Kevlar lines (16 m length and 1 mm diameter). This arrangement positioned the sphere at 15 m with reference to the transducer plate and the counter weight ensured the sphere was stationary relative to the platform. The transducer plate was adjusted in real-time following a pre-programmed sequence of angles. The sequence of angles was programmed to extend beam coverage across the target for $B(\alpha, \beta)$ measurements (Figure 2d). The orientation of the transducer plate was precisely measured by absolute encoders (model: Gurley A19, accuracy: $\pm 0.04°$), and recorded as the alongships (major) and athwartships (minor) mechanical angles.

Table 1. Manufacturer specifications of the transducers used in this study.

Transducer	MSI-38	Simrad ES38-DD	Simrad ES120-7CD
f (kHz)	38	38	120
Serial number	100-0602	28362	109
$\alpha_{-3\ \mathrm{dB}}' \setminus \beta_{-3\ \mathrm{dB}}'$ (°)	14	7.4\7.5	7.4\7.3
Ψ' (dB re 1 sr)	−14.7	−20.2	−20.3
Λ' (electrical°/geometric°)	–	21.9	23

In addition to the DeCAF deployments (Figure 1), the transducers and general purpose transceivers (GPTs) were routinely installed on an acoustic optical system (AOS) (EP 2013) and a profiling lagrangian acoustic optical system (PLAOS) (IN 2015-C02 and IN 2017-V02) for evaluating depth-dependent repeatability in calibrated G_0. The platform based calibration data acquisition settings are tabulated in Table 2.

The AOS is a self-contained multi-frequency acoustic optical platform equipped with 38 (ES38-DD) and 120 kHz (ES120-7CD) split-beam transducers and GPTs (Ryan *et al.*, 2009; Sherlock *et al.*, 2010). The platform attaches to the headline of the commercial fishing vessel's demersal trawlnet (Ryan and Kloser, 2016). Prior to calibration, the AOS was detached from the trawlnet and vertically deployed down to 800 m (with stopovers at 100 m intervals). A 38.1 mm diameter WC sphere (at 20 m) was suspended beneath the transducers by a thin (0.5 mm) monofilament line (no counter weight attached).

The PLAOS is a profiling multi-frequency acoustic optical platform equipped with 38 (MSI-38), 120 (ES120-7CD), and 333 kHz (ES333-7CD) split-beam transducers and GPTs operable down to 1500 m (Kloser *et al.*, 2016; Marouchos *et al.*, 2016). Two WC spheres of diameter 22 (at 4.5 m) and 38.1 mm (at 5.5 m) were suspended concurrently underneath the transducers by a thin (0.5 mm) monofilament line. The 38 kHz transducer was calibrated with a 38.1 mm WC, and the 120 kHz was calibrated with a 22 mm WC sphere.

The AOS and PLAOS were not designed to tilt the transducer mounting plate (as in DeCAF) thus the $B(\alpha, \beta)$ measurements were not performed. These calibrations are used to compare the depth-dependent G_0 variations derived using the DeCAF system and to examine repeatability of TS measurements over the deployments.

Split-beam echosounder calibration

In a Simrad EK60 split-beam echosounder, the data from each transmission (ping) includes received echo power p_{er} (W), phase angles α and β (°) (in two orthogonal alongships and athwartships planes typically aligned with major and minor transducer axes respectively), with the GPT settings: frequency f (kHz), transmit power p_{et} (W), pulse duration τ (s), G_0, area backscattering coefficient s_a ($\mathrm{m}^2\ \mathrm{m}^{-2}$) correction factor $S_{a\ \mathrm{corr}}$ (dB re 1) (i.e. difference in energy of the nominal and actual received pulses), and Ψ of the transducer. These data and associated settings were used to calculate TS (Figure 2b) and volume backscattering strength S_v (dB re 1 $\mathrm{m}^2\ \mathrm{m}^{-3}$) as

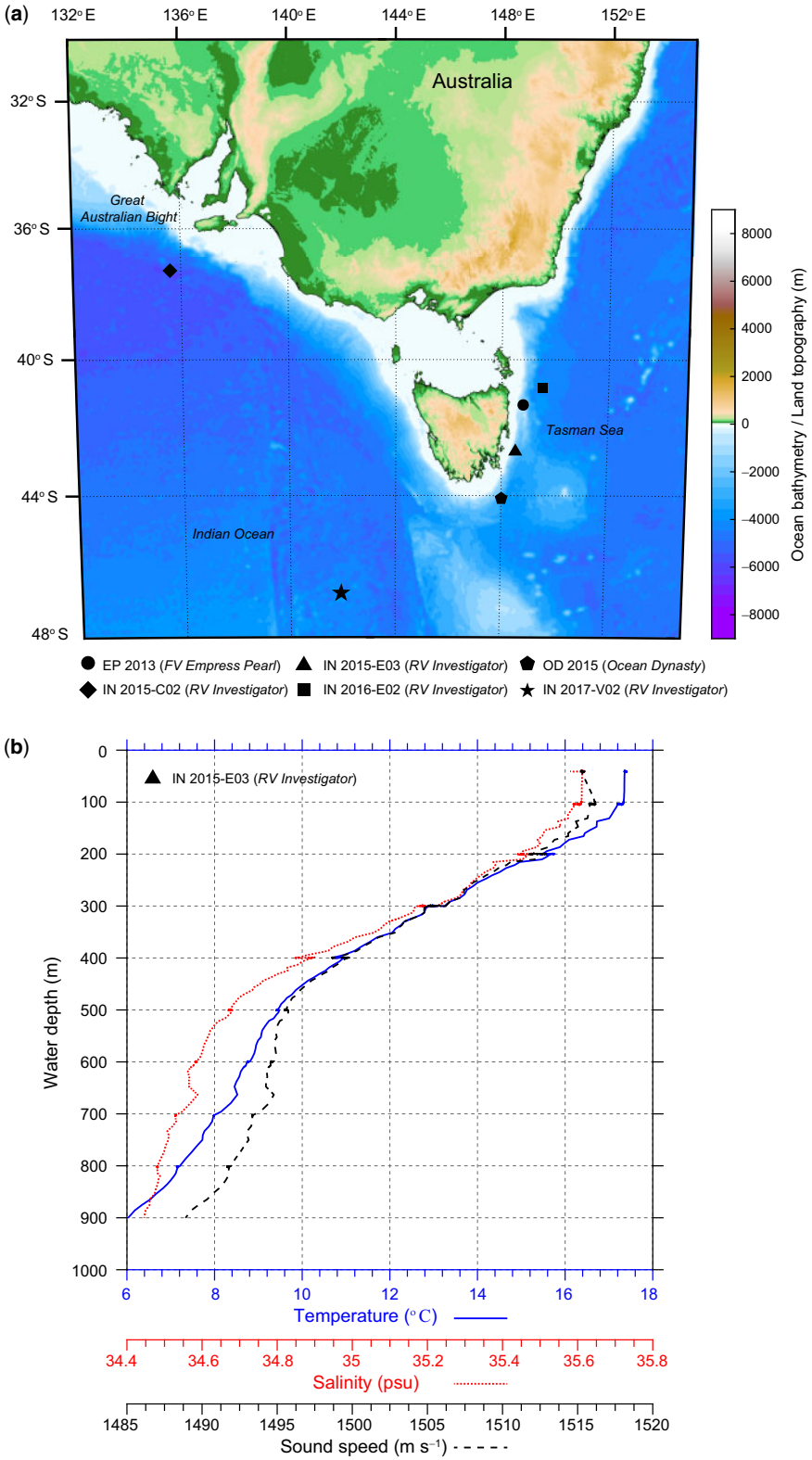

Figure 1. Map in the top panel shows geographic location and year of calibration deployments using DeCAF, AOS, and PLAOS. The bottom panel displays environmental conditions at the deployment site (IN 2015-E03). The environmental parameters were measured during all deployments and utilized in the respective calibration analyses.

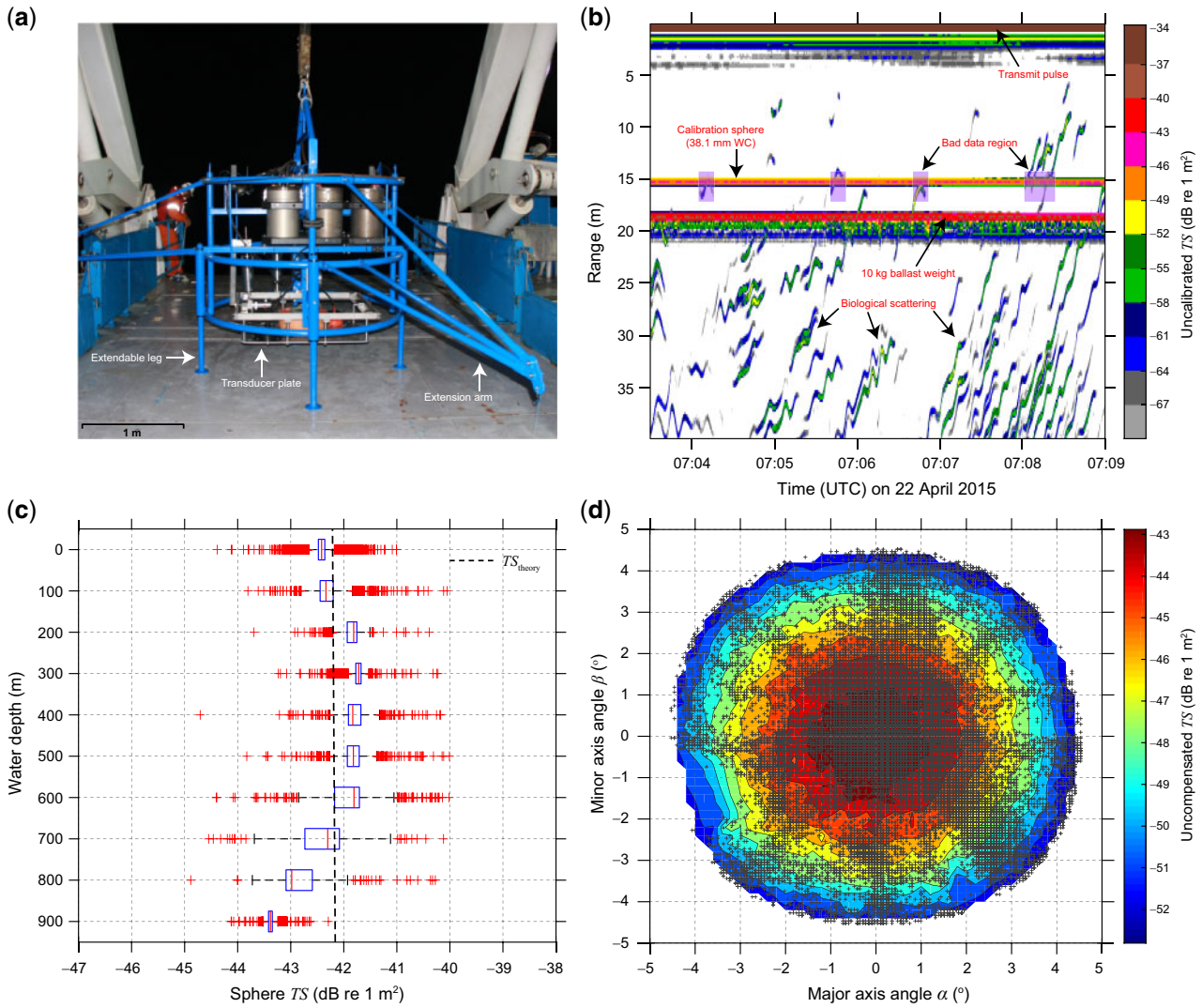

Figure 2. (a) The DeCAF platform with extension arms on board *RV Investigator* (IN 2015-E03). Panel (b) displays an example of 38 kHz (ES38-DD) *in situ* uncalibrated *TS* echogram with platform at 300 m. It is important to isolate sphere *TS* region (at 15 m) from all other possible sources of interference including biological scattering flagged as bad data. The resulting near-axis [$B(\alpha,\beta) \leq 0.3$ dB] calibrated *TS* as a function of water depth is depicted in panel (c). The corresponding $B(\alpha,\beta)$ characteristic of the transducer is shown in panel (d). The "+" symbol denotes position (α and β) of the calibration sphere with respect to the electrical major and minor transducer axes at all depths.

$$TS = P_{er} + 40\log_{10}(r) + 2\alpha_a r - 10\log_{10}\frac{(p_{et}\lambda^2 g_0^2)}{16\pi^2} - 20\log_{10}\left(\frac{g(\alpha,\beta)}{g_0}\right), \text{ and} \quad (1)$$

$$S_v = P_{er} + 20\log_{10}(r) + 2\alpha_a r - 10\log_{10}\left(\frac{(p_{et}\lambda^2 g_0^2 c_w \tau \psi)}{32\pi^2}\right) - 2S_{a\ \mathrm{corr}}, \quad (2)$$

where P_{er} (dB re 1 W) is the received power, r (m) is the range to the target, α_a (dB m^{-1}) is the absorption coefficient, λ (m) is the wavelength, g_0 (dimensionless) is the transducer on-axis gain, $g(\alpha,\beta)$ (dimensionless) is the transducer gain in the direction of off-axis angles α and β (°), c_w (m s^{-1}) is the sound speed in water, and ψ (sr) is the equivalent two-way beam angle (Demer *et al.*, 2015).

The transducer gain $g(\alpha,\beta)$ is defined as the ratio of acoustic intensity values observed at a distant point, resulting from transmissions with constant transmit electric power of a real transducer and an idealized lossless omnidirectional transducer [see Equation (1.5) in Demer *et al.* (2015)]. The transducer on-axis gain g_0 is the $g(\alpha,\beta)$ on the transducer beam axis ($\alpha = \beta = 0$) that has been logarithmically transformed and denoted in this paper as G_0. ψ is the solid angle at the apex of the ideal conical beam which would produce the same echo-integral as the real transducer when the targets are randomly distributed in space [see Equation (2.11) in Simmonds and MacLennan (2005)]. In this paper, ψ is expressed in decibel as $\Psi = 10\log_{10}(\psi)$.

Split-beam transducers are separated into subarrays of piezoelectric elements (e.g. four quadrants for the circular transducers used in this study). The effective separation between the subarray centres (d_{eff}) cause resolvable range differences to the target that are observed as phase-differences ϕ_e (electrical°) in the received

Table 2. Platform based calibration data acquisition settings.

Platform	DeCAF			AOS		PLAOS	
Transducer model	ES38-DD	MSI-38	ES120-7CD	ES38-DD	ES120-7CD	MSI-38	ES120-7CD
f (kHz)	38	38	120	38	120	38	120
p_{et} (W)	2000	500	500[a]	2000	500[a]	500	250[a]
τ (ms)	1.024	1.024	1.024	1.024	1.024	0.512	0.256

[a]Following the manufacturer's recommendation, 500 W transmit power was used for ES120-7CD transducer calibrations on DeCAF and AOS. With reference to the numerical simulation results reported by Pedersen (2006), this transmit power may possibly cause a 0.3 dB non-linear sound attenuation for 120 kHz in seawater (at 9 m distance from the sound source). To reduce non-linear effects in 120 kHz, the transmit power was decreased for PLAOS calibration as recommended by Korneliussen *et al.* (2008).

signals between each pair of quadrants. The split-beam echosounder estimates α and β from ϕ_e as

$$\phi_e = \Lambda \sin\theta, \tag{3}$$

where θ (geometric°) is the angle to the target relative to the transducer beam axis (i.e. α or β). The symbol Λ (electrical°/geometric°) is termed as the transducer angle sensitivity, a factor used to convert split-beam electrical angles to target bearing angles in alongships (major) and athwartships (minor) planes. The Λ can also be represented as the product of acoustic wavenumber k (m^{-1}) and d_{eff}. The α and β of the sphere position were used to model the transducer $B(\alpha, \beta)$ as

$$B(\alpha,\beta) = 6.0206\left(\left(\frac{2\alpha}{\alpha_{-3\,\mathrm{dB}}}\right)^2 + \left(\frac{2\beta}{\beta_{-3\,\mathrm{dB}}}\right)^2 - 0.18\left(\frac{2\alpha}{\alpha_{-3\,\mathrm{dB}}}\right)^2\left(\frac{2\beta}{\beta_{-3\,\mathrm{dB}}}\right)^2\right), \tag{4}$$

where $\alpha_{-3\,\mathrm{dB}}$ and $\beta_{-3\,\mathrm{dB}}$ (°) denotes the along- and athwartships –3 dB beamwidths of the transducer. Equation (2.6) in Demer *et al.* (2015) has been logarithmically transformed and presented here as Equation (4). This equation (after applying angle offsets) was used to compensate the recorded *TS* measurements for angular location in the acoustic beam. In this paper, the $B(\alpha, \beta)$ compensated sphere *TS* derived from received power signals is referred to as the "compensated *TS*", while the recorded *TS* without applying $B(\alpha, \beta)$ compensation is denoted as the "uncompensated *TS*".

Accurate computation of Ψ essentially requires precise sphere position information (α and β) that has to be measured completely independent of the split-beam angle information. Accordingly, the transducer mounting plate in DeCAF was rotated in two axes (Figure 3a) to characterize $B(\alpha, \beta)$ of the transducer. In order to compute Ψ of transducers experimentally, the sphere *TS* data were recorded from the on-axis main lobe to a level less than –6 dB down in both α (major) and β (minor) directions of the transducer axes (Figure 3d). The α and β recorded by the DeCAF were converted from Cartesian to polar coordinate to represent the transducer $B(\alpha, \beta)$ as a function of mechanical angle off-axis (Figure 3e). A polynomial fit to the resulting distribution was utilized to calculate the half power points and the corresponding beamwidth $\theta_{-3\,\mathrm{dB}}$ (°). The Ψ was calculated by two methods, first, by integrating the $B(\alpha, \beta)$ as a function of mechanical angles off-axis [see Equation (2) in Reynisson (1998)], and second using an empirical formula (Urick, 1983). For a circular transducer with >99% of the transmitted energy confined within the main lobe, the Ψ can be computed as

$$\Psi = 10\log_{10}\left(\frac{(\theta_{-3\,\mathrm{dB}})^2}{5800}\right). \tag{5}$$

The manufacturer-specified Ψ' values were recalculated based on the difference in sound speed at the deployment site (Figure 1b) to compare with the *in situ* measurements (Foote, 1987; Bodholt, 2002). The tank temperature data for MSI-38 transducer was unknown, therefore the Ψ' values were calculated assuming a summer time tank temperature of 20 (°C).

In the calibration process (Figure 4), the G_0 were adjusted to compensate for the discrepancy observed between the on-axis *TS* and TS_{theory} (recalculated for the environmental conditions at each depth) as

$$\text{new } G_0 = \frac{TS - TS_{\mathrm{theory}}}{2} + \text{old } G_0, \tag{6}$$

where new G_0 and old G_0 (dB re 1) represents calibrated and uncalibrated G_0 respectively (Figure 3f). The established depth-dependent non-linear changes in the recorded sphere *TS* (Figure 2c) were characterized by a polynomial variation in new G_0 (Ryan *et al.*, 2009; Ryan and Kloser, 2016). This polynomial function was integrated in the analyses to calibrate *in situ TS* at each depth. It is important to note that ±1 dB change in the derived new G_0 represents a twofold ±2 dB variation in the recorded *TS* data. The $S_{a\ \mathrm{corr}}$ were calculated at each depth using standard methods to test for variability and provide calibrated S_v measurements (Demer *et al.*, 2015).

Echosounder calibrations are normally valid for near on-axis measurements if the $B(\alpha, \beta)$ compensation is correct. For PLAOS calibrations, adequate care was taken to position the sphere close to the acoustic axis of all transducers. The alignment of the transducers were adjusted to obtain sufficient overlap of acoustic footprints at the sphere range [see Figure 1 in Kloser *et al.* (2016)]. Moreover, measurement of $\theta_{-3\,\mathrm{dB}}$ parameters using the DeCAF system characterized the transducer $B(\alpha, \beta)$, and the calibration analyses were performed ensuring appropriate $B(\alpha, \beta)$ compensation (Figure 4).

The calibration data files were processed using a custom *Matlab-Echoview* software (Echoview, 2015) suite that was developed to facilitate the analyses. The single target detection (split-beam method 2 algorithm) parameters defined in *Echoview* were:

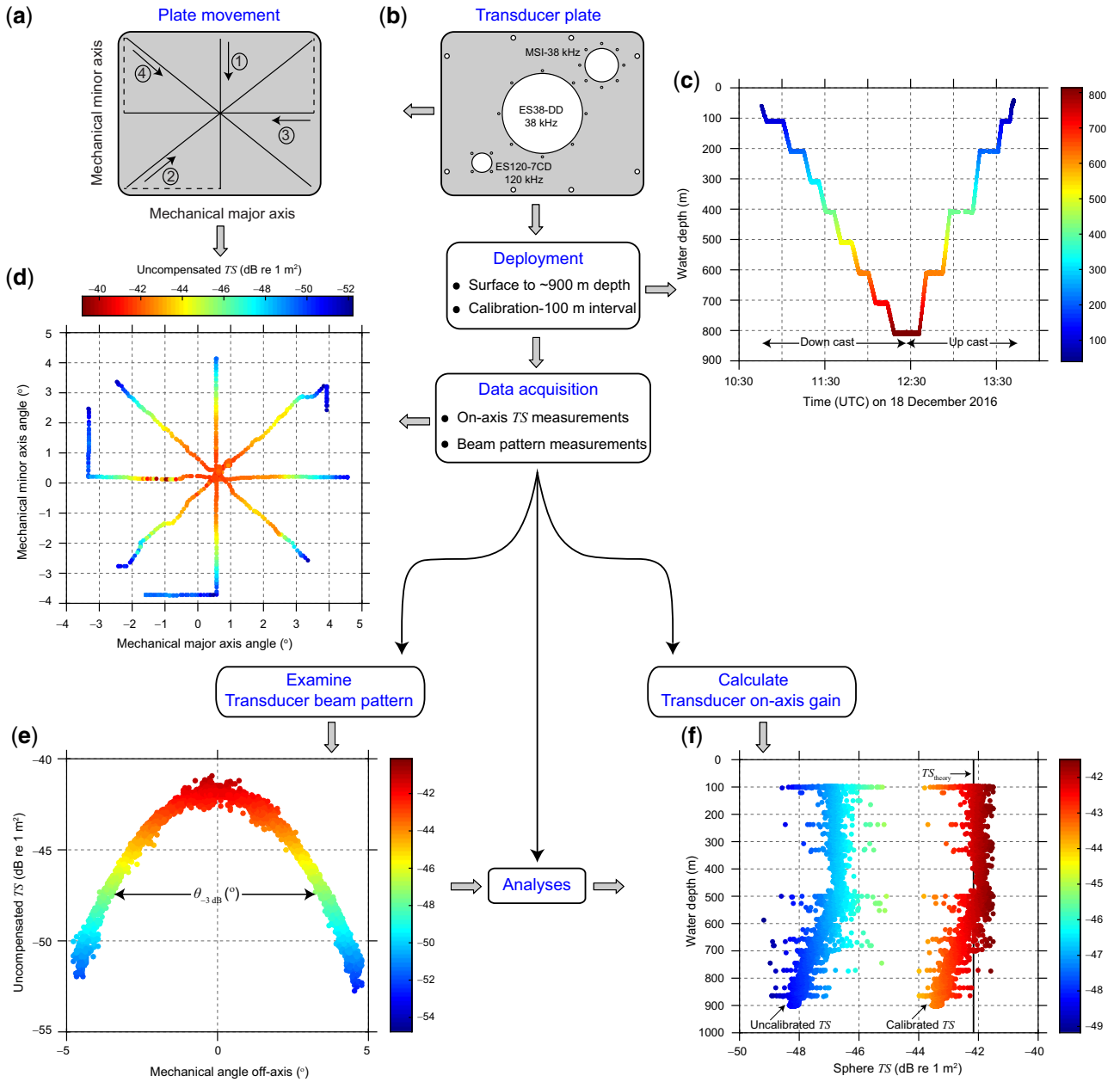

Figure 3. Represents graphical abstract of the methodology implemented in this study. The DeCAF platform was deployed from the surface down to 800 m, with calibration stopovers at 100 m depth intervals as in panel (c). The transducer plate was adjusted in real-time following a sequence of angles illustrated in panel (a) for on-axis *TS* and $B(\alpha, \beta)$ measurements [panel (d)]. The recorded data were used for calibration analyses to examine the transducer $B(\alpha, \beta)$ characteristics [panel (e)] and new G_0 [panel (f)].

–50 (dB re 1 m^2) *TS* threshold; 6 (dB re 1 m^2) pulse length determination level (i.e. the decibel level below the peak value of a detected pulse defined for determining the pulse length during single target detection); 0.3 (dimensionless) minimum normalized pulse length, 1.5 (dimensionless) maximum normalized pulse length (normalized pulse length is the ratio of measured and transmitted pulse length intended to reject pulses that fail the estimate for expected pulse length); and 12 dB maximum beam compensation parameter [i.e. the compensation applied to a recorded *TS* value to correct it for the transducer $B(\alpha, \beta)$]. The resulting sphere *TS* data were processed within *Matlab* using a graphical user interface (GUI). The GUI enabled the user to dynamically adjust parameters (such as *TS* limits and depth ranges) to export results in a systematic way.

Results

Depth-dependent new G_0 variation

The new G_0 of each transducer over multiple deployments highlights distinct variation with depth (Figure 5). The new G_0 (between 20 and 1000 m) varied by 0.7 ± 0.3, 1.1 ± 0.2, and 0.3

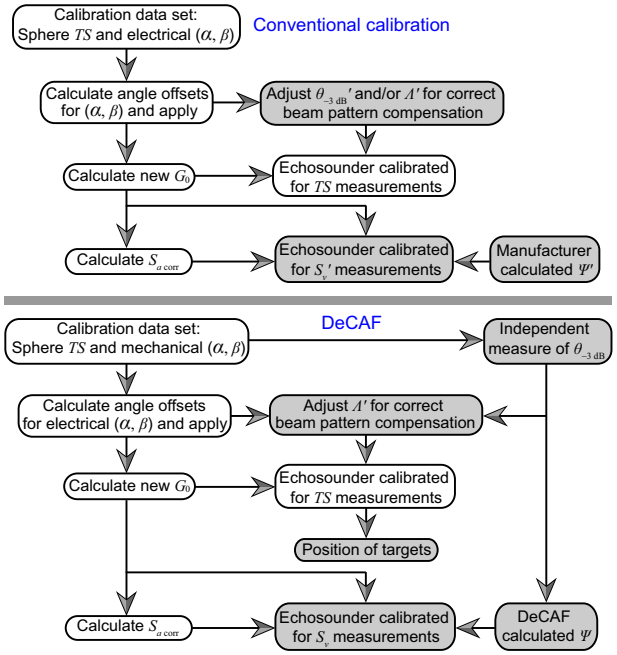

Figure 4. Flowchart of the calibration analyses for unbiased *TS* measurements and biomass estimation.

± 0.3 dB, respectively, for ES38-DD, MSI-38, and ES120-7CD transducers, indicating significant correlation with depth. The associated correlation coefficients (r) are –0.86, 0.95, and 0.96 (with p-values < 0.001). Opposite correlations of new G_0 values (–0.86 and 0.95) with a broader depth-dependent new G_0 variations are evident for ES38-DD (range: 23.6–24.3 dB) and MSI-38 (range: 18.7–19.8 dB) transducers. The ES120-7CD (exclusive of the outliers) displays relatively stable variation that is positively correlated (0.96) within a narrower range of new G_0 values (range: 27.3–27.6 dB).

The precision of new G_0 representing relative variability or repeatability of *TS* measurements at each depth including down and up casts are summarized in Table 3. The variability in new G_0 is greater at the water surface for all the transducers where the temperature variations (±2°C) between the calibration deployments are highest (Figure 6).

The difference in new G_0 calculated for respective down and up calibration profiles highlight the magnitude of depth hysteresis (Figure 7). The hysteresis values were within ±0.2 dB for all the transducers, representing a twofold ±0.4 dB (9%) variation in the recorded *TS* data. This hysteresis effect is not consistent between transducers, indicating unique pressure/temperature response and tolerance of the transducers varying as a function of depth/temperature.

The derived $S_{a\ corr}$ (between 20 and 1000 m) varied by 0.2 ± 0.1, 0.1 ± 0.1, and 0.1 ± 0.03 dB, respectively, for ES38-DD, MSI-38, and ES120-7CD transducers. The associated r values are 0.24 (p =0.47), –0.43 (p =0.17), and 0.11 (p =0.74), indicating stable depth-dependent variation and not significantly correlated with depth.

Calculated Ψ of the transducers

The Ψ values calculated by integrating the $B(\alpha, \beta)$ (as a function of mechanical angles) and using the empirical formula (Equation

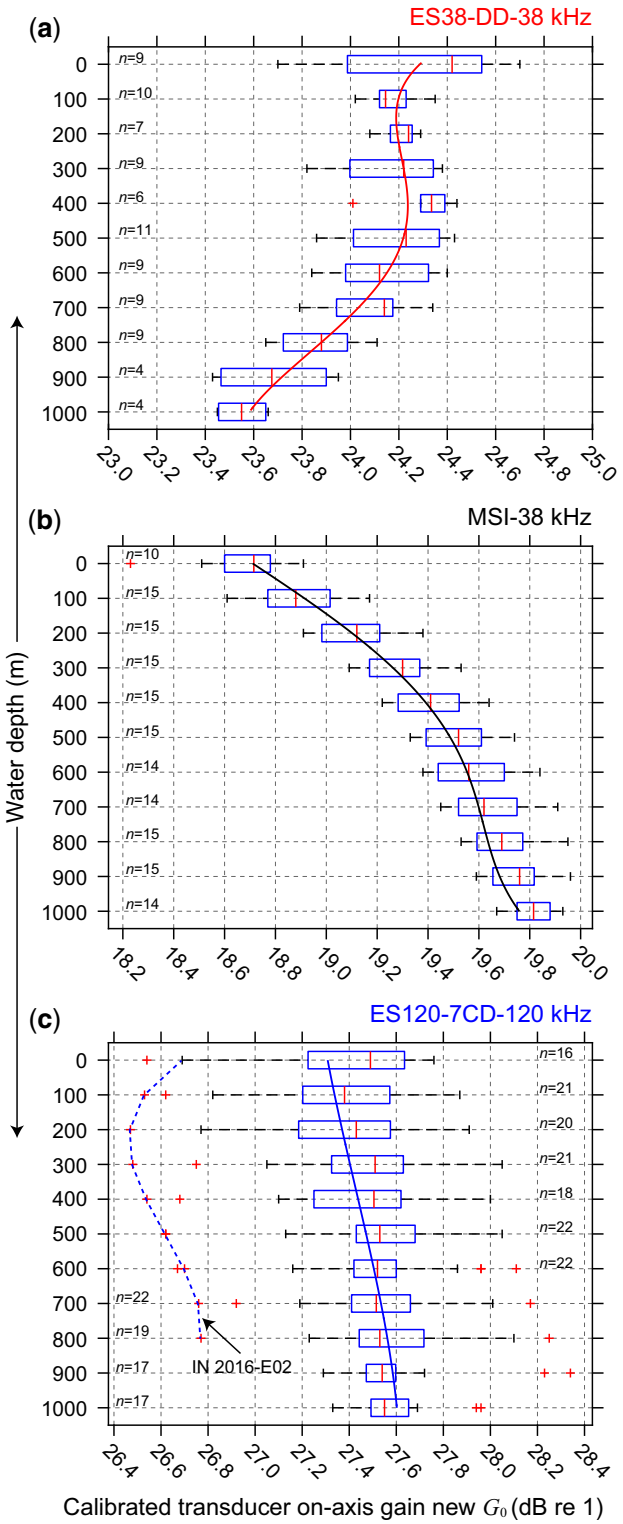

Figure 5. Box plot represents repeatability in new G_0 for (a) ES38-DD, (b) MSI-38, and (c) ES120-7CD transducers. A polynomial fit to the average new G_0 values with number of deployments (n) at each depth are superimposed. It is important to note that ±1 dB change in the new G_0 represents a twofold ±2 dB variation in the recorded *TS* data [see Equation (6)]. Correspondingly, the 120 kHz sphere *TS* acquired during IN 2016-E02 was nearly –2 dB less sensitive as compared with the remaining deployments.

5) were similar between the methods with a maximum difference of 0.02 dB. The calculated Ψ (between 20 and 800 m) varied by 0.3 ± 0.3, 0.4 ± 0.4, 0.4 ± 0.3 dB, respectively, for ES38-DD, MSI-38, and ES120-7CD transducers, indicating relatively stable depth-dependent variation but high standard deviation of measurements (Figure 8, Table 4). The associated r values are 0.68 (p =0.04), 0.62 (p =0.07), and –0.58 (p =0.10). The Ψ is expected to vary with the change in sound speed with depth (1520–1485 m s^{-1}). This would introduce a negative 5% (~0.2 dB) change (r = –0.96, p < 0.001) in Ψ with depth as the sound speed decreases (Figure 8). Therefore, the correlation observed in the 120 kHz transducer is consistent with this expected variation while the two 38 kHz transducers display positive correlation with depth but none are statistically significant.

Table 3. Summary of calibration parameters describing precision in new G_0.

	Precision in new G_0 (dB)					
Depth	***n***	**ES38-DD**	***n***	**MSI-38**	***n***	**ES120-7CD**
0	9	24.29 ± 0.29	10	18.67 ± 0.14	16	27.35 ± 0.29
100	10	24.17 ± 0.06	15	18.87 ± 0.13	21	27.33 ± 0.28
200	7	24.21 ± 0.04	15	19.10 ± 0.11	20	27.37 ± 0.26
300	9	24.16 ± 0.17	15	19.27 ± 0.11	21	27.44 ± 0.26
400	6	24.30 ± 0.10	15	19.40 ± 0.10	18	27.42 ± 0.27
500	11	24.19 ± 0.18	15	19.49 ± 0.10	22	27.49 ± 0.25
600	9	24.15 ± 0.17	14	19.56 ± 0.11	22	27.49 ± 0.23
700	9	24.08 ± 0.14	14	19.61 ± 0.10	22	27.52 ± 0.22
800	9	23.88 ± 0.12	15	19.67 ± 0.09	19	27.57 ± 0.21
900	4	23.68 ± 0.22	15	19.73 ± 0.08	17	27.60 ± 0.19
1000	4	23.55 ± 0.10	14	19.81 ± 0.06	17	27.58 ± 0.12

Precision represents relative repeatability of *TS* measurements over the calibration deployments (in Figure 1). The number of deployments (n) at each depth are also tabulated.

The Ψ of transducers calculated using the DeCAF system were consistently lower than the Ψ' values specified by the manufacturer at all depths. Of note is the ES38-DD transducer where the calculated Ψ at 600 m is 0.85 dB less than the specified Ψ' value, and represents a first-order bias in biomass estimate (Figure 8, Table 4). In a typical deep-water biomass survey (between 400 and 800 m), the differences in Ψ values would result in the corrected survey S_v being 18 ± 2, 6 ± 1, 5 ± 2% higher than the measured S_v with the same increase in estimated biomass, respectively, for ES38-DD, MSI-38, and ES120-7CD transducers.

Unbiased *TS* measurements

Inaccurate values of new G_0 will translate to biased *TS*. Similarly, errors in Λ and/or $\theta_{-3\,\mathrm{dB}}$ cause incorrect angular position of the

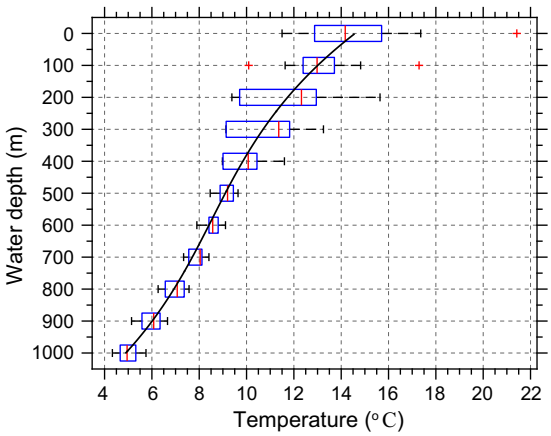

Figure 6. Observed temperature variations between the calibration deployments (in Figure 1). The average values at each depth are overlaid.

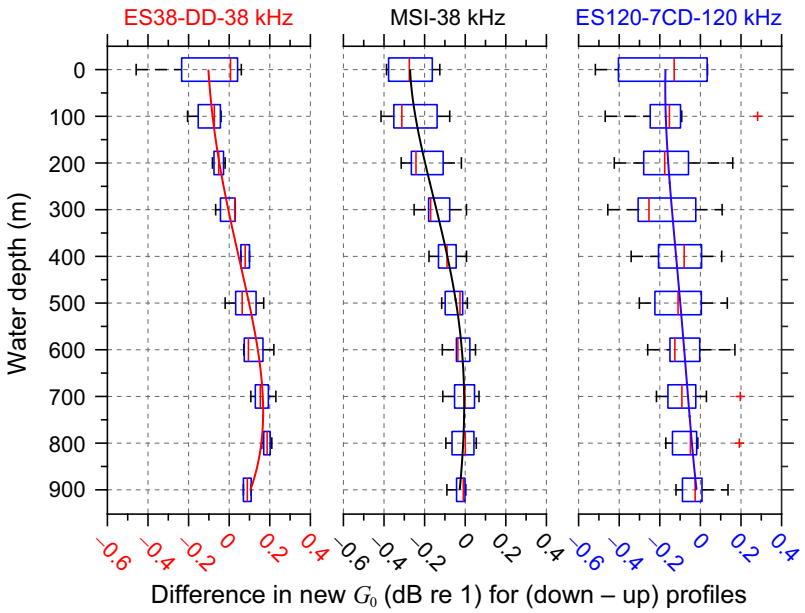

Figure 7. Difference in new G_0 for respective down and up calibration profiles representing the magnitude of depth hysteresis associated with each transducer. A polynomial fit to the average values at each depth are overlaid.

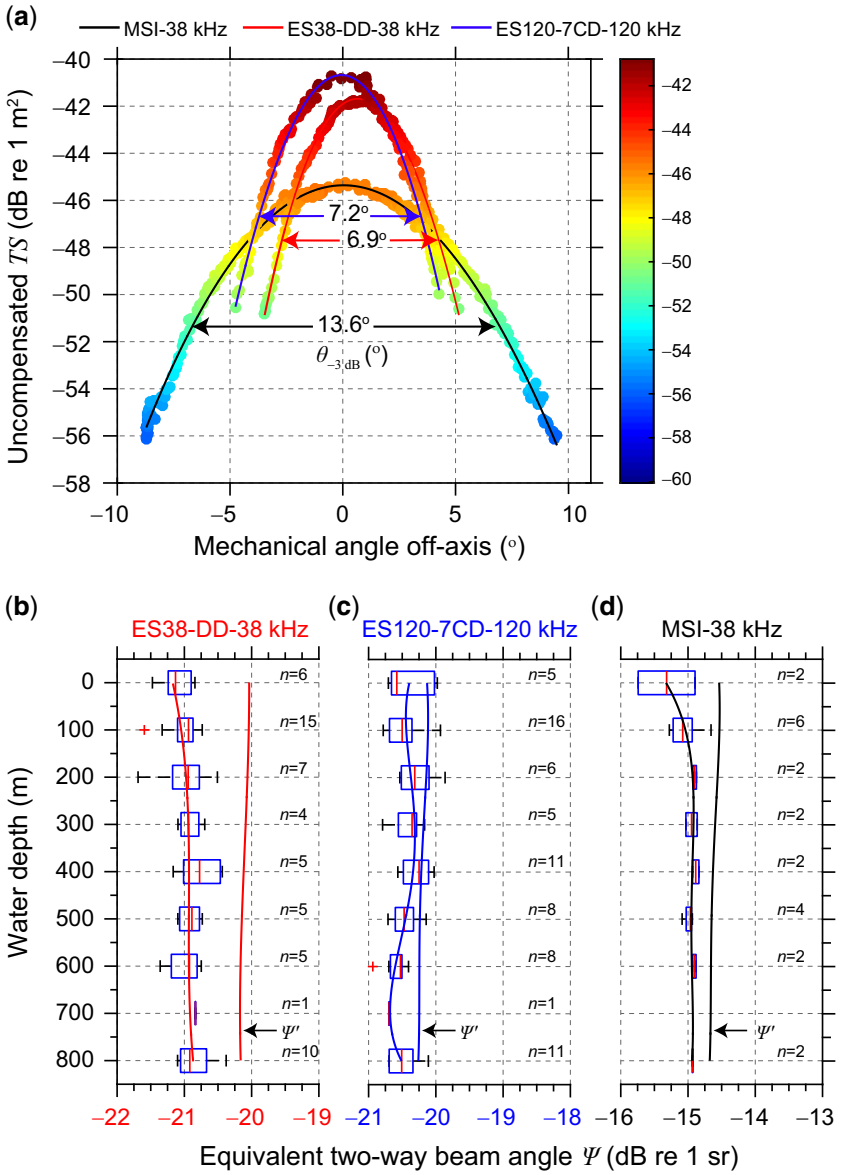

Figure 8. (a) Two-way $B(\alpha, \beta)$ characteristics of the transducers are represented as a function of DeCAF mechanical angles off-axis. The box plots represent depth vs. Ψ variation for (b) ES38-DD, (c) ES120-7CD, and (d) MSI-38 transducers. A polynomial fit to the average Ψ values with number of $B(\alpha, \beta)$ measurements (n) at each depth are superimposed. The manufacturer-specified Ψ' values (adjusting for the difference in sound speed) are juxtaposed to assess accuracy.

targets (α and β) and potentially compensated off-axis *TS*. The consequences are demonstrated in Figure 9 considering MSI-38 transducer as an example. Due to practical constraints, the MSI-38 calibration data were acquired using Simrad ES38-12 GPT settings. The ES38-12 has nominal 12.5° $\theta_{-3\,\mathrm{dB}}'$ and 12.5 Λ' (electrical°/geometric°). Consequently, the compensated *TS* data for MSI transducer does not exhibit a uniform response across the transducer axes, evidencing inappropriate Λ and/or $\theta_{-3\,\mathrm{dB}}$ used during the data acquisition. The *TS* display significant bias in $B(\alpha, \beta)$ compensation (~2 dB for 10° off-axis angles, note that the magnitude of this bias would be different in other transducers). Independent measurement of MSI-38 transducer $B(\alpha, \beta)$ using the DeCAF system resolved the ambiguity in $\theta_{-3\,\mathrm{dB}}$ (hence Ψ), and the off-axis *TS* measurements are corrected by adjusting the Λ' value (Figure 9). Accordingly, the accurate Λ (10.5) required to provide an unbiased *TS* response of the MSI transducer is recomputed with 13.5° $\theta_{-3\,\mathrm{dB}}$ measured using the DeCAF system ($\theta_{-3\,\mathrm{dB}}$ values were averaged for this purpose). The calculated Λ also vary with the change in sound speed with depth (1520–1485 m s^{-1}). This would introduce a positive 0.2 (electrical°/geometric°) change in Λ with depth as the sound speed decreases.

Discussion

Echosounder on-axis sensitivity

The contrasting behaviour of depth-dependent new G_0 values and hysteresis presumably indicates the consequence of both temperature and pressure-induced effects on the transducers. The active bottom surfaces of ES38-DD, MSI-38, and ES120-7CD transducers have approximate diameters of 450, 200, and

Table 4. Summary of calibration parameters describing accuracy of Ψ.

Depth	Accuracy of Ψ (dB)											
	ES38-DD				MSI-38				ES120-7CD			
	n	Ψ	Ψ'	Bias	n	Ψ	Ψ'	Bias	n	Ψ	Ψ'	Bias
0	6	−21.12 ± 0.17	−20.03	28%	2	−15.32 ± 0.42	−14.54	19%	5	−20.39 ± 0.31	−20.13	6%
100	15	−21.01 ± 0.18	−20.03	25%	6	−15.04 ± 0.19	−14.54	12%	16	−20.48 ± 0.18	−20.12	8%
200	7	−21.01 ± 0.28	−20.04	25%	2	−14.90 ± 0.03	−14.56	8%	6	−20.27 ± 0.19	−20.14	3%
300	4	−20.92 ± 0.13	−20.08	21%	2	−14.95 ± 0.08	−14.60	8%	5	−20.42 ± 0.17	−20.18	5%
400	5	−20.76 ± 0.25	−20.12	15%	2	−14.89 ± 0.05	−14.64	5%	11	−20.29 ± 0.18	−20.22	1%
500	5	−20.91 ± 0.13	−20.14	19%	4	−14.99 ± 0.05	−14.65	8%	8	−20.46 ± 0.16	−20.24	5%
600	5	−21.00 ± 0.20	−20.15	21%	2	−14.91 ± 0.03	−14.66	5%	8	−20.59 ± 0.13	−20.24	8%
700	1	−20.84	−20.15	17%	0	–	−14.67	–	1	−20.69	−20.25	10%
800	10	−20.83 ± 0.22	−20.16	16%	2	−14.93 ± 0.00	−14.68	5%	11	−20.50 ± 0.17	−20.26	5%

Accuracy indicates the closeness of calculated Ψ with respect to the manufacturer-specified Ψ' value (recalculated based on the difference in sound speed at the deployment site). The related first-order change (%) in biomass estimation with number of $B(\alpha, \beta)$ measurements (n) at each depth are also tabulated.

152 mm, respectively. The transducers are constructed as arrays of piezoelectric elements with different composition and manufacturing standards. The elements are moulded into housings designed to withstand high hydrostatic pressure. Conceivably, each transducer possesses a unique temperature and pressure response (with different tolerance) that could distinctively differ as a function of depth. A complete assessment of temperature and pressure-induced effects on transducers (including impedance measurements and related new G_0 variation) is beyond the scope of the present study. In this study, we accentuate the requirement to measure on-axis sensitivity of echosounders over the range of environmental conditions that exist in the survey area, ideally before and after the survey.

It is also possible over time that the performance of transducers and associated electronic components may degrade gradually or abruptly. The transducers are also vulnerable to mechanical damage and ageing effects (Knudsen, 2009). Therefore, it is important to quantify such changes routinely to apply suitable corrections required during the post-processing of data and subsequent species identification and biomass estimation. An abrupt shift in the new G_0 (as in Figure 5c) indicates a system change and necessitates more frequent calibrations to monitor performance.

Variability in on-axis sensitivity has been observed by other researches from a combination of factors including: system electronics (Jech *et al.*, 2005); ageing effects (Knudsen, 2009); data acquisition settings (power, pulse length, and non-linear effects) (Tichy *et al.*, 2003; Pedersen, 2006); range to the calibration sphere (Ona *et al.*, 1996); signal-to-noise ratio (Kieser *et al.*, 2005); environmental conditions (pressure, temperature, and hysteresis) (Kloser, 1996; Demer and Renfree, 2008); density and composition of the calibration sphere (Foote and MacLennan, 1984; Islas-Cital *et al.*, 2010); and position (α and β) of the target sphere within the acoustic beam (Kieser *et al.*, 2000).

Demer and Renfree (2008) demonstrated that temperature can cause impedance variation and potentially affect the transducer performance. However, in our deep-water applications involving DeCAF, AOS, and PLAOS, the new G_0 (and related *TS*) vary significantly due to combined temperature and pressure-induced effects on the transducer. In the similar context, Kloser (1996) calibrated a towed (EDO Western 38 kHz) transducer from the surface down to 1000 m and evaluated depth-dependent changes in the transducer sensitivity and $B(\alpha, \beta)$. The towed transducer exhibited a 3 dB depth-dependent variance in the sphere *TS* with a hysteresis of (∼1 dB at 700 m) for the respective down and up calibration deployments. Dalen *et al.* (2003) deployed dual-frequency deep-towed Simrad ES38-DD and ES120-7DD transducers down to 500 m and noticed a 2 dB difference in the resulting sphere *TS*. Ryan *et al.* (2009) calibrated an AOS down to 900 m and observed a 1 and 6 dB shift in the sphere *TS* response of the ES38-DD and ES120-7D respectively. The ES120-7D transducer used by Ryan *et al.* (2009) is now discontinued by the manufacturer. Likewise, O'Driscoll *et al.* (2013) calibrated the ES38-DD transducer on an AOS down to 600 m and observed a 0.6 dB difference in new G_0, representing a 1.2 dB variation in the recorded *TS* data.

The hysteresis observed by Kloser (1996) was most likely due to the air-backed design of the transducer used. Whereas, the Simrad ES38-DD used in this study is fabricated as a liquid filled transducer, whilst the MSI-38 and Simrad ES120-7CD utilize composite transducer technology. These transducers have greatly reduced hysteresis (<0.5 dB) and seem more suitable for deep-water applications.

Accuracy of Ψ

Accuracy of Ψ is an important factor in echo-integration based biomass estimation. It is common practice to assume that the manufacturer-specified (calibrated) Ψ', adjusting for the sound speed variation is correct due to the difficulty in obtaining an independent measurement of the transducer $B(\alpha, \beta)$. The Ψ of transducers calculated using the DeCAF system at all depths are consistently lower than the values specified by the manufacturer. Similar results were also reported earlier by Reynisson (1998) while analysing the Ψ values derived for 18 individual hull-mounted transducers. Therefore, considering the differences observed between calculated Ψ and Ψ' values, it is important to determine the true value of Ψ for each transducer *in situ* to reduce bias in biomass estimation. Based on the present study results it appears there are no significant depth-dependent Ψ changes for the transducers evaluated. For these transducers, at least an independent $B(\alpha, \beta)$ measurements at the water surface revealed the accuracy of Ψ, and indicate the related first-order corrections needed for biomass estimates. Of course it would be preferable to test all transducers at their depth of operation for

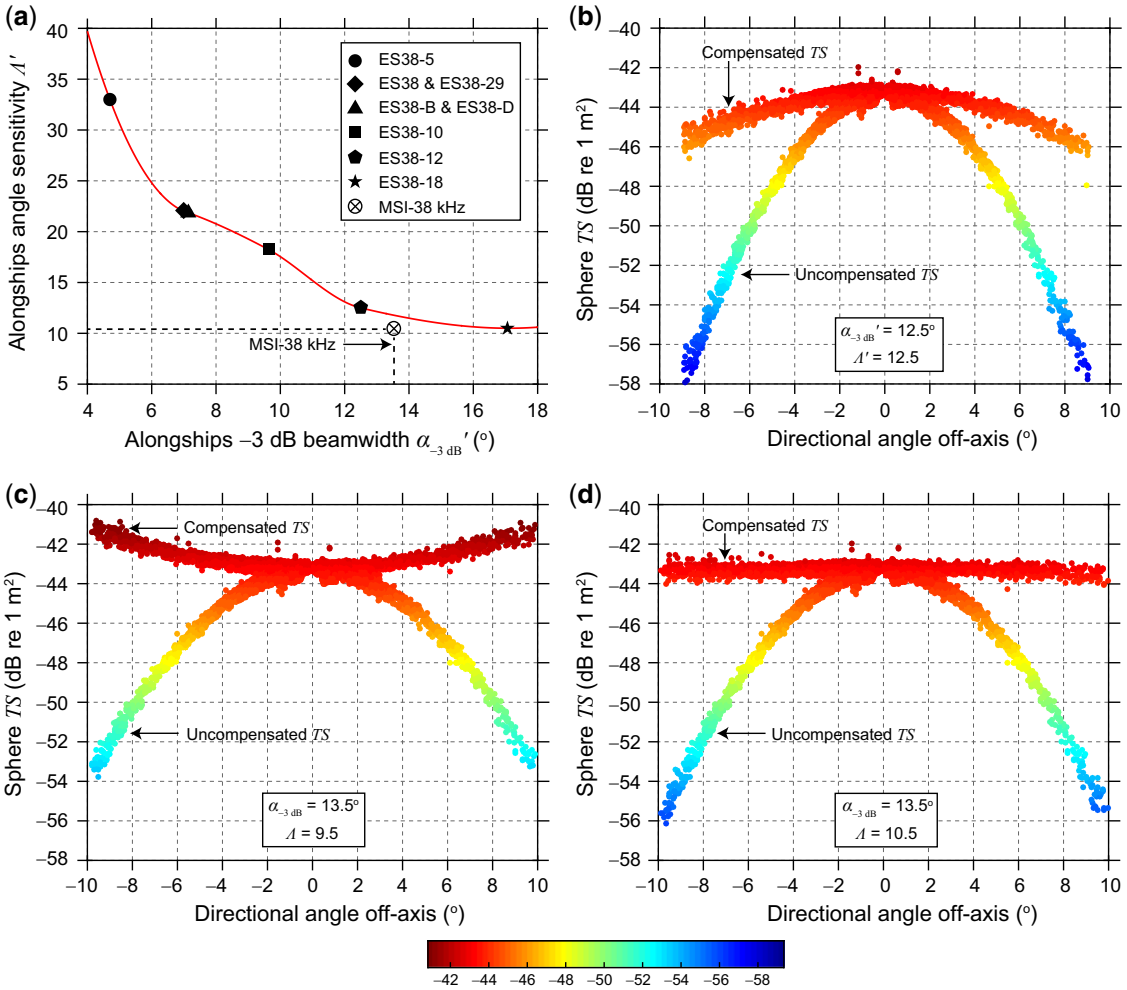

Figure 9. Panel (a) represents the relationship between nominal alongships $\alpha_{-3\,\mathrm{dB}}{}'$ and Λ' of commonly used Simrad 38 kHz transducers. The $\alpha_{-3\,\mathrm{dB}}{}'$ values broadly exhibit an inverse correlation with the Λ' (particularly for narrow-beam transducers). The ES38-12 GPT settings (shown in figure) were used to acquire the MSI-38 calibration data, displaying inadequate $B(\alpha, \beta)$ compensation [panel (b)]. Using 13.5° $\theta_{-3\,\mathrm{dB}}$ measured by the DeCAF system as a constant parameter, the accurate Λ value required to generate an unbiased *TS* response across the off-axis angles is practically determined as depicted in panel (c) and (d).

any changes to surface values through monitoring the correct $B(\alpha, \beta)$ compensation of the off-axis sphere *TS*.

Jech *et al.* (2005) measured the alongships $\theta_{-3\,\mathrm{dB}}$ of a ES38-12 transducer, and observed a difference of 0.6° compared with the manufacturer's nominal value. This reduced the calculated Ψ by 0.3 dB, although the difference was within the nominal specified range of ±1 dB provided by the manufacturer. In this study, the Ψ' values specified in the calibration sheets of the transducers were used and precision of the calculated Ψ' were not provided. Therefore, we recommend the manufacturer to provide precision of the calculated Ψ' for each transducer tested and supplied including the sound speed measured at the transducer face. Jech *et al.* (2005) further demonstrated the influence of threshold on Ψ calculation using the $B(\alpha, \beta)$ integration method. In the present study, the Ψ values were computed with a –12 dB threshold using both integration and empirical (Urick, 1983) methods, and are consistent with a maximum difference of 0.02 dB. Also, the $B(\alpha, \beta)$ of the transducer was measured with the survey echosounder that includes both transceiver (Simrad EK60) and transducer configuration as used for the biomass surveys. The $B(\alpha, \beta)$ is directly measured (using sphere calibration method) as the combined transmit-receive intensity response of the transducer with an independent mechanical angle measurement.

Improving target identification with accurate positioning

Accurate computation of new G_0 and $\theta_{-3\ \mathrm{dB}}$ are needed to obtain unbiased *TS* and position measurements. Ideally, the off-axis sphere *TS* are compensated to an on-axis reference value ensuring correct $B(\alpha, \beta)$ compensation (Figure 4). However, in practice, even after determining accurate $\theta_{-3\,\mathrm{dB}}$, the compensated *TS* measurements across the transducer axes can exhibit a non-uniform response with inaccurate Λ values. The Λ' values specified by the manufacturer should change if the measured $\theta_{-3\,\mathrm{dB}}$ is different from the manufacturer-specified $\theta_{-3\,\mathrm{dB}}{}'$. Minor error in Λ' values can cause incorrect angular position of targets within the beam and major biases in the compensated off-axis *TS* measurements. Rectification of this error is advantageous for unbiased *TS* studies (Ona, 1999), particularly involving multi-frequency

acoustic-optical platforms (such as AOS and PLAOS), wherein the acoustics and optics are often used for coincident measurements of the targets [see Figure 10 in Kloser *et al.* (2016)]. For accurate target positioning, we assume any phase delay induced errors in the transmission and reception circuitry are compensated for by adjusting the Λ parameter to match phase angles with the mechanically measured angles. In this case, the Λ is "matched" to the survey echosounder that should be documented and monitored to note any changes between calibrations. This could be indicative of changes in the system and subsequent changes to the perceived $B(\alpha, \beta)$ and Ψ.

Influence of calibration parameters on biomass estimation

Inaccurate values of new G_0 and Ψ can translate to a bias in an echo-integration based biomass estimation (Demer, 2004; Simmonds and MacLennan, 2005). In recent years, multi-frequency deep-water acoustic platforms have been used for improved species identification (Kloser *et al.*, 2002, 2013, 2016) and biomass estimation (Kloser *et al.*, 1996; Ryan and Kloser, 2016), necessitating accurate calibration of each echosounder at the operating depth. For such studies, it is important to characterize the depth-dependent variations in new G_0 and accuracy of Ψ as both parameters have a direct impact on biomass estimation (Figure 4).

Normally, echosounders are calibrated at the water surface or in a controlled laboratory environment. However, the new G_0 value obtained at the surface (or in a calibration tank) is inapplicable for deep-water systems if the recorded *TS* varies as a function of depth (Kloser, 1996; Dalen *et al.*, 2003; Ryan *et al.*, 2009; Pedersen *et al.*, 2011; O'Driscoll *et al.*, 2013). As an example, the average new G_0 value of ES38-DD at 600 m was less sensitive when compared with the surface new G_0 and would result in a 6% decrease in the estimated biomass, conversely, the MSI-38 at 600 m was more sensitive resulting in a 50% increase in the estimated biomass. Similarly, an imprecise Ψ can introduce significant first-order bias in biomass estimation. In this case, the manufacturer-specified Ψ' for ES38-DD transducer (recalculated based on the sound speed variation) at 600 m depth was significantly larger (0.85 dB) than the calculated Ψ. In a deep-water biomass survey and analyses, using the manufacturer-specified Ψ' would decrease the estimated biomass by 18%.

Depending on the characteristic response of an individual transducer used for the survey, inaccurate values of new G_0 and Ψ in combination could contribute to substantial bias (when not counterbalancing each other) in biomass estimation. Therefore, calibrations of echosounders at the surveying depth are needed to determine accurate new G_0, and validation of the correct Ψ at the surface and preferably at depth for new transducers.

Conclusion

Considering the diverse applications of deeply deployed multi-frequency acoustic platforms for species identification, classification, and biomass survey, this work demonstrates the importance of accurate deep-water calibration to reduce the bias in estimates of biomass and to improve species identification. Three transducers (Simrad ES38-DD, ES120-7CD, and MSI-38) were selected to examine the depth-dependent repeatability in new G_0 and accuracy of Ψ. The results indicate appreciable variations in new G_0 and Ψ that in combination can result in significant systemic biases in quantitative biomass estimation.

In order to improve calibration of acoustic systems it is recommended that

(1) The new G_0 of each transducer is quantified over the range of environmental conditions (i.e. temperature, salinity, and pressure) encountered during the biomass survey (ideally before and after the survey).

(2) The manufacturer-specified Ψ' needs to be recalculated with the survey echosounder and monitored under actual environmental conditions. At a minimum, independent $B(\alpha,\beta)$ measurements at the water surface should be performed to reveal the accuracy of Ψ.

(3) The manufacturer needs to provide a transducer calibration report specifying the precision of Ψ' and the sound speed measured at the transducer face.

Acknowledgements

The authors are grateful to Gordon Keith for his invaluable support in developing the calibration GUI. We are thankful to Andreas Marouchos, Matthew Sherlock, Dave Kube, Jeff Cordell (and the team members of CSIRO Engineering and Technical Services) for their kind support provided during the DeCAF design and data acquisition. We wish to express our appreciation to the officers and crew (including CSIRO MNF team) in charge for the respective scientific voyages. The authors express their gratitude to the editor and the reviewers for their meticulous remarks to improve the manuscript. This project was supported by CSIRO Oceans and Atmosphere.

References

Bodholt, H. 2002. The effect of water temperature and salinity on echo sounder measurements. *In* ICES Symposium on Acoustics in Fisheries 2002-Montpellier. 1–7 pp.

Brede, R., Kristensen, F. H., Solli, H., and Ona, E. 1990. Target tracking with a split-beam echo sounder. Rapports et Procès-Verbaux des Réunions du Conseil International pour l'Exploration de la Mer, 189: 254–263.

Brierley, A., Goss, C., Watkins, J., and Woodroffe, P. 1998. Variations in echosounder calibration with temperature, and some possible implications for acoustic surveys of krill biomass. CCAMLR Science, 5: 273–281.

Brierley, A. S., Saunders, R. A., Bone, D. G., Murphy, E. J., Enderlein, P., Conti, S. G., and Demer, D. A. 2006. Use of moored acoustic instruments to measure short-term variability in abundance of Antarctic krill. Limnology and Oceanography: Methods, 4: 18–29.

Dalen, J., and Bodholt, H. 1991. Deep towed vehicle for fish abundance estimation concept and testing. ICES C.M. 1991/B: 53. 1–13 pp.

Dalen, J., Nedreaas, K., and Pedersen, R. 2003. A comparative acoustic-abundance estimation of pelagic redfish (Sebastes mentella) from hull-mounted and deep-towed acoustic systems. ICES Journal of Marine Science, 60: 472–479.

Demer, D., Berger, L., Bernasconi, M., Bethke, E., Boswell, K., Chu, D., Domokos, R., et al. 2015. Calibration of acoustic instruments. ICES Cooperative Research Report No. 326. 133 pp.

Demer, D., and Hewitt, R. 1992. Calibration of an acoustic echo-integration system in a deep tank, with system gain comparisons over standard sphere material, water temperature and time. SC-CAMLR-SSP/9. 127–144 pp.

Demer, D. A. 2004. An estimate of error for the CCAMLR 2000 survey estimate of krill biomass. Deep Sea Research Part II: Topical Studies in Oceanography, 51: 1237–1251.

Demer, D. A., and Renfree, J. S. 2008. Variations in echosounder–transducer performance with water temperature. ICES Journal of Marine Science, 65: 1021–1035.

Doksæter, L., Godø, O. R., Olsen, E., Nøttestad, L., and Patel, R. 2009. Ecological studies of marine mammals using a seabed-mounted echosounder. ICES Journal of Marine Science, 66: 1029–1036.

Echoview. 2015. Echoview 6.1 Acoustic processing software. Echoview Software Pty Ltd. GPO Box 1387 Hobart, Tasmania, Australia, 7001.

Fernandes, P. G., Stevenson, P., Brierley, A. S., Armstrong, F., and Simmonds, E. J. 2003. Autonomous underwater vehicles: future platforms for fisheries acoustics. ICES Journal of Marine Science, 60: 684–691.

Foote, K. G. 1987. Dependence of equivalent beam angle on sound speed. ICES C.M. 1987/B: 2. 1–6 pp.

Foote, K. G., and MacLennan, D. N. 1984. Comparison of copper and tungsten carbide calibration spheres. The Journal of the Acoustical Society of America, 75: 612–616.

Godø, O. R., Sivle, L. D., Patel, R., and Torkelsen, T. 2013. Synchronous behaviour of cetaceans observed with active acoustics. Deep Sea Research Part II: Topical Studies in Oceanography, 98: 445–451.

Godø, O. R., and Totland, A. 1996. A stationary acoustic system for monitoring undisturbed and vessel affected fish behaviour. ICES C.M. 1996/B: 12. 1–11 pp.

Handegard, N. O., Buisson, L. D., Brehmer, P., Chalmers, S. J., De Robertis, A., Huse, G., Kloser, R. et al. 2013. Towards an acoustic-based coupled observation and modelling system for monitoring and predicting ecosystem dynamics of the open ocean. Fish and Fisheries, 14: 605–615.

Islas-Cital, A., Atkins, P., and Foo, K. 2010. Standard target calibration of broad-band active sonar systems in a laboratory tank. *In* OCEANS 2010 IEEE-Sydney, IEEE. 1–10 pp.

Jech, J. M., Foote, K. G., Chu, D., and Hufnagle, L. C. 2005. Comparing two 38-kHz scientific echosounders. ICES Journal of Marine Science, 62: 1168–1179.

Kaartvedt, S., Røstad, A., Klevjer, T. A., and Staby, A. 2009. Use of bottom-mounted echo sounders in exploring behavior of mesopelagic fishes. Marine Ecology Progress Series, 395: 109–118.

Kieser, R., Mulligan, T., and Ehrenberg, J. 2000. Observation and explanation of systematic split-beam angle measurement errors. Aquatic Living Resources, 13: 275–281.

Kieser, R., and Ona, E. 1988. Comparative analysis of split beam data. ICES C.M. 1988/B: 44. 1–16 pp.

Kieser, R., Reynisson, P., and Mulligan, T. J. 2005. Definition of signal-to-noise ratio and its critical role in split-beam measurements. ICES Journal of Marine Science, 62: 123–130.

Kloser, R., Koslow, J., and Williams, A. 1996. Acoustic assessment of the biomass of a spawning aggregation of orange roughy (Hoplostethus atlanticus, Collett) off south-eastern Australia, 1990-93. Marine and Freshwater Research, 47: 1015–1024.

Kloser, R., Ryan, T., Sakov, P., Williams, A., and Koslow, J. 2002. Species identification in deep water using multiple acoustic frequencies. Canadian Journal of Fisheries and Aquatic Sciences, 59: 1065–1077.

Kloser, R. J. 1996. Improved precision of acoustic surveys of benthopelagic fish by means of a deep-towed transducer. ICES Journal of Marine Science, 53: 407–413.

Kloser, R. J., Macaulay, G. J., Ryan, T. E., and Lewis, M. 2013. Identification and target strength of orange roughy (Hoplostethus atlanticus) measured in situ. The Journal of the Acoustical Society of America, 134: 97–108.

Kloser, R. J., Ryan, T. E., Keith, G., and Gershwin, L. 2016. Deep-scattering layer, gas-bladder density, and size estimates using a two-frequency acoustic and optical probe. ICES Journal of Marine Science, 73: 2037–2048.

Kloser, R. J., Ryan, T. E., Young, J. W., and Lewis, M. E. 2009. Acoustic observations of micronekton fish on the scale of an ocean basin: potential and challenges. ICES Journal of Marine Science, 66: 998–1006.

Knudsen, H. P. 2009. Long-term evaluation of scientific-echosounder performance. ICES Journal of Marine Science, 66: 1335–1340.

Korneliussen, R. J., Diner, N., Ona, E., Berger, L., and Fernandes, P. G. 2008. Proposals for the collection of multifrequency acoustic data. ICES Journal of Marine Science, 65: 982–994.

Malan, J., Marouchos, A., Sherlock, M., Ryan, T., and Kloser, R. 2016. Deep water acoustic calibration facility: Development of a platform. *In* OCEANS 2016-Shanghai, IEEE. 1–5 pp.

Marouchos, A., Sherlock, M., Kloser, R., Ryan, T., and Cordell, J. 2016. A profiling acoustic and optical system (pAOS) for pelagic studies; Prototype development and testing. *In* OCEANS 2016-Shanghai, IEEE. 1–6 pp.

Moline, M. A., Benoit-Bird, K., O'Gorman, D., and Robbins, I. C. 2015. Integration of scientific echo sounders with an adaptable autonomous vehicle to extend our understanding of animals from the surface to the bathypelagic. Journal of Atmospheric and Oceanic Technology, 32: 2173–2186.

O'Driscoll, R. L., Oeffner, J., and Dunford, A. J. 2013. In situ target strength estimates of optically verified southern blue whiting (Micromesistius australis). ICES Journal of Marine Science, 70: 431–439.

Ona, E. 1990. Optimal acoustic beam pattern corrections for split beam transducers. ICES C.M. 1990/B: 30 Sess.R. 1–12 pp.

Ona, E. 1999. Methodology for target strength measurements. ICES Cooperative Research Report No. 235. 59 pp.

Ona, E. 2003. An expanded target-strength relationship for herring. ICES Journal of Marine Science, 60: 493–499.

Ona, E., Zhao, X., Svellingen, I., and Foote, K. G. 1996. Some pitfalls of short-range standard-target calibration. ICES C.M.1996/B: 36. 1–18 pp.

Ona, E., and Vestnes, G. 1985. Direct measurements of equivalent beam angle on hull-mounted transducers. ICES C.M. 1985/B: 43. 1–10 pp.

Patel, R., Handegard, N. O., and Godø, O. R. 2004. Behaviour of herring (Clupea harengus L.) towards an approaching autonomous underwater vehicle. ICES Journal of Marine Science, 61: 1044–1049.

Pedersen, A. 2006. Effects of nonlinear sound propagation in fisheries research. PhD dissertation, University of Bergen, Norway. 307 pp.

Pedersen, G., Godø, O. R., Ona, E., and Macaulay, G. J. 2011. A revised target strength–length estimate for blue whiting (Micromesistius poutassou): implications for biomass estimates. ICES Journal of Marine Science, 68: 2222–2228.

Reynisson, P. 1986. A comparison of two methods for measuring the equivalent beam angles of hull mounted transducers (preliminary). ICES C.M. 1986/B: 17. 1–14 pp.

Reynisson, P. 1990. A geometric method for measuring the directivity of hull-mounted transducers. Rapports et Procès-Verbaux des Réunions du Conseil International Pour l'Exploration de la Mer, 189: 176–182.

Reynisson, P. 1998. Monitoring of equivalent beam angles of hull-mounted acoustic survey transducers in the period 1983–1995. ICES Journal of Marine Science, 55: 1125–1132.

Ryan, T. E., and Kloser, R. J. 2016. Improved estimates of orange roughy biomass using an acoustic-optical system in commercial trawlnets. ICES Journal of Marine Science, 73: 2112–2124.

Ryan, T. E., Kloser, R. J., and Macaulay, G. J. 2009. Measurement and visual verification of fish target strength using an acoustic-optical system attached to a trawlnet. ICES Journal of Marine Science, 66: 1238–1244.

Sherlock, M., Ryan, T., and Kloser, R. 2010. A combined acoustic and optical instrument for fisheries studies. *In* OCEANS 2010 IEEE-Sydney, IEEE. 1–5 pp.

Simmonds, E. 1984. A comparison between measured and theoretical equivalent beam angles for seven similar transducers. Journal of Sound and Vibration, 97: 117–128.

Simmonds, E. 1990. Very accurate calibration of a vertical echo sounder: a five-year assessment of performance and accuracy. Rapports et Procès-Verbaux des Réunions du Conseil International pour l'Exploration de la Mer, 189: 183–191.

Simmonds, J., and MacLennan, D. N. 2005. Fisheries acoustics: theory and practice, Blackwell Science. 437 pp.

Tichy, F. E., Solli, H., and Klaveness, H. 2003. Non-linear effects in a 200-kHz sound beam and the consequences for target-strength measurement. ICES Journal of Marine Science, 60: 571–574.

Urick, R. J. 1983. Principles of underwater sound. McGraw-Hill Book Company, New York.

Urmy, S. S., Horne, J. K., and Barbee, D. H. 2012. Measuring the vertical distributional variability of pelagic fauna in Monterey Bay. ICES Journal of Marine Science, 69: 184–196.

Vagle, S., Foote, K., Trevorrow, M. V., and Farmer, D. M. 1996. A technique for calibration of monostatic echosounder systems. IEEE Journal of Oceanic Engineering, 21: 298–305.

Handling editor: David Demer